Accurate and Consistent Microwave Observations of Venus and their Implications

Bryan J. Butler
National Radio Astronomy Observatory [1]
P. O. Box O
Socorro, NM 87801

Paul G. Steffes, Shady H. Suleiman
School of Electrical and Computer Engineering
Georgia Institute of Technology
Atlanta, GA 30332–0250

Marc A. Kolodner
Johns Hopkins University
Applied Physics Laboratory
Laurel, MD 20723–6099

Jon M. Jenkins
Search for Extraterrestrial Intelligence Institute
NASA Ames Research Center
Moffett Field, CA 94035

submitted to Icarus on August 31, 2000

38 pages; 3 figures (1 color); 4 tables.

[1]The National Radio Astronomy Observatory is a facility of the National Science Foundation operated under cooperative agreement by Associated Universities, Inc.

Proposed running head: Venus Microwave Spectrum

Please address all editorial correspondence to:

Bryan J. Butler
National Radio Astronomy Observatory
P. O. Box O
Socorro, NM 87801

phone: 505-835-7261
FAX: 505-835-7027
email: bbutler@nrao.edu

Abstract

We present observations of Venus at four frequencies: 4.86, 8.44, 14.94, and 22.46 GHz. These were obtained with the Very Large Array (VLA), and calibrated in a consistent fashion. The brightness temperature of Venus at the four frequencies is derived, and compared to emission models which contain elements of the atmosphere, surface, and subsurface of Venus. A single model can fit the data, but there is a slight problem at the longer wavelengths (somewhat unrealistic subsurface model parameters must be used). Improvements in this model over past models include new formalisms for the microwave opacity of SO_2 and H_2SO_4, and incorporation of measured topography and surface characteristics from Magellan. A model which fits the presented data includes a sensible pressure temperature profile, a disk averaged abundance of gaseous H_2SO_4 of 2.5 ppm at and just below the lower cloud layer and an average SO_2 abundance of 40 ppm for all altitudes below the cloud layers. This H_2SO_4 abundance is consistent with the values inferred from Magellan occultations, taking into account the differences between equatorial and polar locations (Jenkins and Steffes 1991; Kolodner and Steffes 1998). The SO_2 abundance in the lower atmosphere is in agreement with earlier results of Steffes *et al.* (1990), but much lower than the 180 ppm inferred from the Pioneer sounder probe (Oyama *et al.* 1980) or the 130 ppm inferred from infrared observations (Bézard *et al.* 1993).

Keywords: Venus, Radio Observations

Introduction

Since telescopes were first pointed at the heavens, Venus has been the object of intense scrutiny by intrigued astronomers. For some time, it was not known that what was being observed was not the surface of the planet, but actually bright clouds at the top of a very thick atmosphere. In fact, at optical wavelengths, no radiation from the surface or atmosphere below the clouds, either scattered or emitted, can be observed. However, they may be probed at the much longer wavelengths of the radio portion of the spectrum. Thus, it was not until the development of receivers and telescopes sensitive to radiowaves (in the late 1950's and early 1960's) that the thick lower atmosphere and surface of Venus were probed (see Barrett and Staelin [1964] for a good review of early radio observations of Venus). Since that time, many such observations have been undertaken, allowing our knowledge of these regions of Venus to continually progress. It has recently become known that there are also windows in the infrared, through which the lower atmosphere, and even the surface, may be probed (Allen and Crawford 1984; Crisp *et al.* 1991; Lecacheux *et al.* 1993). In addition to Earth–based observations, several spacecraft have visited Venus, balloons have been released into its atmosphere (Blamont *et al.* 1995), probes dropped through its atmosphere (Sieff 1991), and landers have been sent to its surface (Vinogradov *et al.* 1976; Florenskii *et al.* 1982). The most recent of those missions was the incredibly successful Magellan spacecraft (Saunders *et al.* 1992), which mapped the surface of the planet in radio emission (Pettengill *et al.* 1992), radar reflection (Pettengill *et al.* 1991), surface roughness (Tyler *et al.* 1992), and topography (Ford and Pettengill 1992) and helped further characterize the atmosphere

through a number of radio occultation experiments (Steffes *et al.* 1994; Jenkins *et al.* 1994).

Thus, we have built up over time a body of knowledge of what is happening in the lower atmosphere of Venus. The atmosphere is very thick, reaching $\sim$ 90 bars at the surface. It is comprised mostly of CO_2 ($\sim$ 96%), with a small amount of N_2 ($\sim$ 4%), and trace amounts of SO_2, CO_2, H_2O, H_2SO_4, and other gases. Because of the thick atmosphere, and because CO_2 is such a good greenhouse gas, the temperature at the surface is very hot, near 750 K. There are several cloud and haze layers in the atmosphere, between about 30 and 90 km, comprised mostly of sulfuric acid (H_2SO_4). However, important questions still remain unanswered regarding the lower atmosphere of Venus. One of these questions is the abundance of sulfur–bearing molecules, and their possible spatial (both vertical and horizontal) and temporal variation. For example, the abundance of SO_2 at the cloud tops (near 70 km) decreased sharply from 1978 to 1980, then decreased slowly until 1986, but has held relatively steady since that time (Esposito *et al.* 1988; Na *et al.* 1990; Zasova *et al.* 1993; Na *et al.* 1994). This is in direct contrast to observations which indicate that the abundance of SO_2 in the deep atmosphere (near 40 km) has remained nearly constant over that same time period (Bézard *et al.* 1993). Because SO_2 provides significant opacity at microwave wavelengths, very accurate measurements at those wavelengths, combined with accurate lab measurements of its opacity, and a radiative transfer model for the atmosphere, may be used to provide constraints on its abundance in the lower atmosphere. Observations performed in 1987 (Steffes *et al.* 1990) indicated that the abundance of SO_2 in the deep atmosphere was much lower than measured by the Pioneer sounder (Oyama *et al.* 1980), or subsequently in the infrared by Bézard *et al.* (1993). These differences have not been resolved. Occultation

experiments also seem to indicate that there is some spatial and temporal variation in the abundance of H_2SO_4 in the lower atmosphere (Jenkins and Steffes 1991). Note however that very little is currently known about the vertical distribution of SO_2 and H_2SO_4 in the lower atmosphere.

Recently, accurate lab measurements have provided much improved formalisms for the microwave opacity of SO_2 and H_2SO_4 vapor (Suleiman *et al.* 1996; Kolodner and Steffes 1998). Therefore, we have undertaken a series of interoferometric radio wavelength observations of Venus from the Very Large Array, in an attempt to further understand the lower atmosphere of Venus, and especially the inventory and variability (spatial and temporal) of sulfur-bearing molecules. This paper will describe the first portion of the reduction of those data, including the data collection and calibration, and present average brightness temperature values and their implications. Detailed analysis of maps made from the data will be presented in a future paper (Jenkins *et al.* 2000). There is a well developed history of interferometric observations of Venus (see e.g., Clark and Spencer 1964; Clark and Kuz'min 1965; Berge and Greisen 1969; Hall and Branson 1971; Berge *et al.* 1972; Sinclair *et al.* 1972; Muhleman *et al.* 1973; Pettengill *et al.* 1988; Gurwell *et al.* 1995), but we feel that the improved sensitivity of the observations, the fact that they are based upon a common calibration scale, and the new laboratory information on the microwave opacities of SO_2 and H_2SO_4, warrant this investigation.

Observations and Data Reduction

All observations described herein were undertaken at the Very Large Array (VLA) of the National Radio Astronomy Observatory. The VLA is a collection of 27 radio antennas, each 25 m in diameter, spread out in a Y shape on the plains of San Augustin, New Mexico. Each of the pairs of antennas acts as a two element interferometer, and the combination of all of these individual interferometers allows for the reconstruction of the full sky brightness distribution, in both dimensions (Thompson *et al.* 1991).

The VLA is tunable in eight discrete frequency bands from about 70 MHz to about 50 GHz. We present in this paper measurements in four of these bands: C (4.86 GHz), X (8.44 GHz), U (14.94 GHz), and K (22.46 GHz). A much more complete data set, including more observations at these four frequencies, and data from lower and higher frequencies is in hand, and awaits full analysis. In all of our observations, we observed in the continuum mode, which essentially provides measurements of the total intensity (Stokes I) with an equivalent bandwidth of $\sim$ 92 MHz [2]. The observations were undertaken on different days in April of 1996. Table I lists the dates, along with other experiment and ephemeris information. Calibration of the data proceeded in the normal fashion for VLA data, in the AIPS reduction package. Observations of an unresolved secondary calibrator (see Table II) were used to remove long timescale (10's of minutes) atmospheric and system fluctuations in the data. For all of the observations the absolute flux density scale was set with an observation of 3C286,

[2]The VLA receivers actually operate in the two orthogonal circular polarizations, with $\sim$ 46 MHz bandwidth in each polarization. Since for Venus, we expect the two circular polarizations to have equal intensity, they are combined into a total intensity polarization (Stokes I), for an effective increase of $\sqrt{2}$ to the bandwidth, yielding $\sim$ 65 MHz equivalent bandwidth. There are also two independent IF's (frequency tuners/filters), which are averaged together for another $\sqrt{2}$ effective increase in bandwidth, to $\sim$ 92 MHz.

with assumed flux density values listed in Table II for the different frequencies. Uncertainties in this flux density scale and implications of the measurements described herein on that scale are discussed later in the paper.

The actual measured quantity of a complex interferometer like the VLA is a sampling of the complex visibility function at the positions of the baselines between each of its antennas. The visibility function is the two dimensional Fourier transform of the sky brightness distribution (see Butler and Bastian [1999] for a description of the expected visibility function for a planet). The individual samples of the visibility function are referred to as visibilities, and are complex quantities (real and imaginary, or amplitude and phase). After the initial calibration, the data product was a set of visibilities for Venus. Two additional steps were necessary to obtain the desired final data product: fully calibrated Venus visibilities. The first was a distance correction. Since, in the longer observations (at 14.94 and 22.46 GHz), the distance of Venus changed by $\sim 0.5\%$ during the course of the observations, it was necessary to effectively adjust all of the visibilities to a common distance. A difference of 0.5% in distance would produce an $\sim 1\%$ difference in the received flux density. So, we adjusted all of the visibilities as if they had been measured at the furthest distance to Venus. This adjustment is a relatively simple one, and is discussed in detail in Butler and Bastian (1999). This adjustment was not performed for the shorter observations, since the distance variation over those short periods would have produced less than 0.1% variation in the received flux density.

The last step was to apply the technique of self–calibration (Cornwell and Fomalont 1999) to the Venus visibilities themselves. This was done in order to remove short timescale

fluctuations (mostly atmospheric) in the data. Self–calibration uses a model of the visibilities to derive antenna based corrections to the visibilities which make them self consistent as a function of time. Both the amplitude and phase may be corrected in this manner, but we corrected only the phase. The model we used was an image made from the visibilities (which was made with the aid of a fit to the visibilities). After self–calibration, the data product is a set of fully calibrated visibilities for Venus. Such visibilities may be used to actually make a map of the sky brightness across the visible disk of Venus. This was done for two of the observations (14.94 and 22.46 GHz), the full description of which is in preparation (Jenkins *et al.* 2000). For the purposes of this paper, we simply wished to obtain an estimate of the total flux density for each of the frequencies. These flux densities could then be converted into average brightness temperatures for the planet at the observed frequencies.

Modeling

Given a set of visibilities for a planet, we wish to derive the total flux density from the planet, which can then be used to calculate the average brightness temperature. The total flux density at frequency ν from any source is obtained by integrating the brightness B_ν over the source:

$$S_\nu = \int\int_{\text{source}} B_\nu(\theta, \psi)\, d\Omega \quad , \tag{1}$$

where θ and ψ are the angular sky coordinates, and $d\Omega$ is the element of solid angle. If we assume that we are in the Rayleigh-Jeans portion of the spectrum (safe for the frequencies and temperatures of interest in this paper), then:

$$B_\nu = \frac{2\,k\,T_b}{\lambda^2} \quad , \tag{2}$$

where k is Boltzmann's constant, T_b is the brightness temperature, and λ is the wavelength. Equation 1 then reduces to:

$$S_\nu = \frac{2\,k}{\lambda^2} \int\int_{\text{source}} T_b(\theta,\psi)\,\sin\theta\,d\theta\,d\psi \quad . \tag{3}$$

Now, for small angles on the sky, $\theta \sim \sin\theta \sim r/D$, for physical distance r from the source center, at distance D. Substituting this into Eq. 3 yields:

$$S_\nu = \frac{2\,k}{\lambda^2}\,\frac{1}{D^2} \int\int_{\text{source}} T_b(r,\psi)\,r\,dr\,d\psi \quad . \tag{4}$$

For a circular source (like Venus) of physical radius R (R is the maximum radius from which emission radiates) this reduces to:

$$S_\nu = \frac{2\,k}{\lambda^2}\,\frac{1}{D^2} \int_0^{2\pi}\int_0^{R} T_b(r,\psi)\,r\,dr\,d\psi \quad . \tag{5}$$

Define the average brightness temperature for the source as:

$$\overline{T_b} = \frac{\int_0^{2\pi}\int_0^{R} T_b(r,\psi)\,r\,dr\,d\psi}{\pi\,R^2} \quad . \tag{6}$$

Note that the effective brightness temperature across the visible disk of Venus must account for the fact that the cosmic microwave background emission is blocked by the planet (i.e., it is the *contrast* of the brightness temperature of Venus with that from the CMB that we are actually measuring). Accounting for this effect, we have for the effective brightness temperature of the planet:

$$T_b' = T_b - T_{CMB} \quad , \tag{7}$$

where T_b is the true brightness temperature of the planet, and T_{CMB} is the cosmic microwave background temperature (2.7 K). Combining all of this, and inverting to solve for

the brightness temperature gives:

$$\overline{T_b} = S_\nu \, \frac{\lambda^2}{2\,k} \, \frac{D^2}{\pi\,R^2} \; + \; T_{CMB} \quad . \tag{8}$$

Note that choosing a value for R is somewhat arbitrary, as long as the same value is used when comparing different observations, and when comparing the average brightness temperature obtained from the observations (Eq. 8) to that from a model of the emission (see appendix A). Following the suggestion of Muhleman *et al.* (1979), we use $R = 6120$ km. We obtain the distances for each of the observations from the very accurate JPL planetary ephemeris (which can be accessed on the web through the Horizons system at http://ssd.jpl.nasa.gov/horizons.html).

Since the VLA does not measure total flux density well, we must attempt to derive the total flux density from the measured visibilities. The total flux density is exactly equivalent to the zero spacing flux density (V_o), or the visibility which would be measured by a pair of antennas with zero separation. Since this is physically impossible, we must somehow use the visibilities which we have measured to estimate V_o. We do this by fitting (in a least squares sense) the measured visibilities to the expected visibility function, allowing V_o, and a shape parameter (to allow for limb darkening) to vary. We assume that the sky brightness is like:

$$T_b(r) = T_o \; \cos^n(r/R) \quad , \tag{9}$$

where T_o is the brightness temperature at the disk center, and n is the limb darkening parameter. Then, defining an apparent radial coordinate $\beta = \hat{R}\sqrt{u^2 + v^2}$ ($\hat{R}$ is the apparent size of Venus), the visibility function $V(\beta)$ can be represented by (Butler and Bastian 1999):

$$V(\beta) = V_o \; \Lambda_\xi(z) \quad , \tag{10}$$

where the Λ function of order ξ ($\xi = 1 + n/2$) and argument z ($z = 2\pi\beta$) is given by:

$$\Lambda_\xi(z) = \Gamma(\xi + 1)\left(\frac{1}{2}z\right)^{-\xi} J_\xi(z) \quad . \tag{11}$$

Note that we do not use this sky brightness distribution function because we expect it to be the precisely exact one, but rather because it allows the visibility function to be analytically defined while still allowing for some limb darkening. Given this expected visibility function, we can fit the measured visibilities to find V_o and n. We do this via a non-linear least squares fit, implemented in the AIPS task OMFIT.

In order to model the total flux density we expect from the planet, we develop a radiative transfer model of the atmosphere and surface of Venus. Along any line of sight which intercepts the atmosphere of Venus, there are three possible sources of radiation: emission from the atmosphere itself, emission from the surface and subsurface, and downward emission from the atmosphere which is reflected from the surface. All three of these mechanisms are treated quite rigorously in the model. The model is described in detail in Appendix A. The major improvements implemented in our model are the new formalisms for the microwave absorption of SO_2 and H_2SO_4, and the use of measured topography and surface properties from Magellan.

Results and Discussion

We performed the fits described above on the data set for each of the four frequencies. Figure 1 shows a plot of the real portion of the measured visibilities against β for the 8.44 GHz data, along with the residuals remaining after the fit. The quality of the fit is quite good, remembering that this is a circularly symmetric model (and hence there are expected

deviations which occur on size scales up to the size scale of the disk - hence the "ringing" in the residuals), and that there are some 35000 individual visibilities (so that if the 1-σ error on each visibility is of order 50 mJy/vis, then the error on V_o might be less than 1 mJy). The data quality and quality of the fits is similar at all frequencies. Table III shows the resultant fit values of V_o and n for all of the observed frequencies, along with the 1-σ uncertainties in these quantities. In all cases, the uncertainty in V_o is dominated by the uncertainty in the absolute flux density calibration scale, as the actual fit uncertainty is extremely small (e.g., the 1-σ uncertainty in the value of V_o for the fit to the 22.46 GHz data was roughly 4 mJy, while even if the uncertainty in the flux density scale is as small as 2%, then the uncertainty in the value of V_o from this is nearly 1.8 Jy). Also shown in that table is the estimate of the disk averaged brightness temperature $\overline{T_b}$ obtained from inversion of Eq. 8. In order to obtain this value it was necessary to make a correction for the resolution of Venus by the primary beam of the VLA antennas. This is a small correction factor in all of our cases, and is explained in detail in Appendix B. Table III also lists an uncertainty for the final derived disk averaged brightness temperatures. These uncertainties are completely dominated by the uncertainty in the absolute flux density calibration scale. We have adopted uncertainties of 2, 2, 3, and 5% for the flux density scale at 4.86, 8.44, 14.94, and 22.46 GHz. A full discussion of these errors is beyond the scope of this paper, but this is the current best estimates of these uncertainties at the VLA (R. Perley, personal communication).

We ran the model (described in detail in Appendix A) for these four frequencies while varying the inputs to the model in order to obtain an acceptable fit to the measured brightness temperature values. We stress here that we have not done a full optimization to find the

absolute *best* inputs to the model - we merely adjusted parameters crudely until reasonable agreement to the measured values was achieved, to demonstrate that it could be done. The input temperature-pressure profile was that from Muhleman *et al.* (1979), which is an extrapolation of the profile inferred from occultation measurements of the Mariner 5 spacecraft. The input SO_2 profile consisted of a uniform 40 ppm at all altitudes below 47 km (the base of the lower cloud layer), decreasing exponentially with a scale height of 3 km above that. The input H_2SO_4 profile was one measured by the Magellan spacecraft near 65° N latitude scaled down by a factor of two. This profile is one from Jenkins *et al.* (1994), but modified with the recent laboratory results of Kolodner and Steffes (1998). The factor of two scaling was selected to provide a profile more representative of lower latitude zones (which represent a major portion of the disk averaged brightness), where we know from the preliminary mapping of the 14.94 and 22.46 GHz data that the abundance of H_2SO_4 is less than at high latitudes (Jenkins *et al.* 1998). The H_2SO_4 profile has non-zero values between 37 and 51 km above the surface (in and below the lower cloud), and peaks at about 2.5 ppm. For the subsurface parameters, we used a value of 10^{-6} cal/cm^2/s for the heat flux (q), a value of 10^{-5} cal/s/cm/K for the thermal conductivity (k), a value of 5×10^{-4} for the loss tangent, a value of 8.0 for the dielectric constant in the lower layer, and an upper layer depth of 10 meters. The value of the heat flux is possibly somewhat high (roughly equal to the Earth's heat flux value), given recent analysis of Magellan data (e.g., McGovern *et al.* 1995) but is within reason. The value for the loss tangent is on the low side, but is possibly within reason, given that the specific loss tangent might be as low as 10^{-3} and that the density of the venusian subsurface might be quite high (and if we presume that

scattering effects are small at these wavelengths). The value of the thermal conductivity is quite low, much lower than might be expected for the hot temperatures in the subsurface (one might expect something more like 3×10^{-4} cal/s/cm/K). We do not claim that this low value for the thermal conductivity is necessarily real, or attempt to justify it, except to say that it is necessary in order to fit the model to the longer wavelength measurements. We also freely admit that this simple subsurface model will not be consistent with longer wavelength measurements than those presented in this paper. The model presented here will produce a brightness temperature which is much too high at the longer wavelengths. This problem with the longer wavelength measurements and modeling of the Venus brightness temperature spectrum has been known for some time and discussed at length elsewhere (e.g. Schloerb *et al.* 1976; Muhleman *et al.* 1973). We cannot resolve this problem in the context of the model or measurements presented here.

Figure 2 shows the brightness distribution maps which were the result of running the model at the four frequencies discussed here, and with the input parameters discussed in the preceding paragraph. Note that these brightness temperature maps were *not* used to derive the final disk averaged brightness temperatures, they were calculated simply to demonstrate visually how the emission changes as the frequency is varied. These 4 maps were created using geometry parameters which are appropriate for the longer wavelength observations on April 30, 1996 (subearth longitude 271.8 E, latitude -5.3, position angle of north pole -4.8, distance .4862 AU). As expected, the shorter wavelengths are dominated by emission from the atmosphere, while the longer wavelengths are dominated by emission from the surface. The one-way opacities at the disk center are: 5.3 at 22.46 GHz; 2.3 at 14.94 GHz; 0.76 at

8.44 GHz; and 0.26 at 4.86 GHz. The weighting functions (see appendix A) at the disk center peak at a distance above the surface (6052 km) of roughly 20 km at 22.46 GHz and 12 km at 14.94 GHz, and peak at the surface for 8.44 and 4.86 GHz. So, at 22.46 GHz, the emission is very uniform, since less than 1% of the emission comes from the surface and we have assumed a uniform atmosphere here (not varying as a function of latitude and longitude). At 14.94 GHz, the highest peaks on the surface just start to become visible - peeking through the dense lower atmosphere with their lower brightness temperature (due to both lower surface temperature and lower emissivity). At the particular geometry shown in Fig. 2, the tall peak just above and to the right of the disk center is Beta Regio (including Rhea and Theia Montes). At 8.44 GHz, more surface detail is seen, again, with higher topographic points exhibiting lower brightness temperatures. At 4.86 GHz, the atmosphere is nearly transparent, and surface features are distinct.

Figure 3 shows a plot of the measured and model disk averaged brightness temperatures at the four frequencies. The model fits the data quite well at all four frequencies (to better than 2% relative error). One could argue that the model *should* fit the data quite well, given the freedom in varying the numerous model input parameters. But, with the exception of the thermal conductivity, all of the model inputs are quite sensible, and in fact most of them are constrained by other measurements. The necessity of using a somewhat nonsensical value for the thermal conductivity (which is really a statement about the *ratio* of the value of the heat flux to that of the thermal conductivity) remains somewhat disconcerting, however. If more reasonable values of the subsurface parameters are used, then the model cannot reproduce the high brightness temperatures at 8.44 and 4.86 GHz. This would then imply that there is

a problem with the measurements (most likely in the assumed absolute flux density scale) or that there is some other problem with the model (most likely some phenomena which is not included in our present model - e.g., subsurface scattering). There has been some discussion in the past regarding the possibility of an error of the order of 5% in the absolute flux density scale of Baars *et al.* (1977) for the calibrator sources 3C286 and 3C295 (which were essentially the sources used by us to fix the flux density scale) around 8 GHz (e.g., Turegano and Klein 1980). We cannot exclude this possibility, but point out that very accurate measurements of these calibrators at the VLA seem to show that the Baars *et al.* values are correct for these secondary calibrators at these frequencies (R. Perley, personal communication).

Summary

Using the VLA as an observing tool and by integrating the most modern information on the microwave absorption properties of potential constituents, we have significantly updated our understanding of the microwave emission spectrum of Venus. The results are consistent with a sensible pressure temperature profile, a disk averaged abundance of gaseous H_2SO_4 of 2.5 ppm at and just below the lower cloud layer and an average SO_2 abundance of 40 ppm for all altitudes below the cloud layers. The H_2SO_4 abundance is consistent with the values inferred from Magellan occultations, taking into account the differences between equatorial and polar locations (Jenkins and Steffes 1991; Kolodner and Steffes 1998). The low SO_2 abundance is in agreement with the earlier results of Steffes *et al.* (1990), but much lower than the 180 ppm inferred from the Pioneer sounder probe (Oyama *et al.* 1980) or the 130 ppm inferred from infrared observations (Bézard *et al.* 1993). A more complete analysis of

all of the Venus data taken at the VLA, including detailed maps and observations at shorter and longer wavelengths, will allow for even further understanding of the lower atmosphere of Venus, and in particular of the sulfur bearing molecules therein.

Acknowledgements

The measurements described in this paper would not have been possible without the expert help of the staff at the VLA, whose aid was greatly appreciated. Discussions with M. Gurwell, D. Muhleman, and G. Orton were extremely helpful. The aid of K. Desai in implementing the AIPS task OMFIT was appreciated. PGS, SHS, and MAK were supported by the NASA Planetary Atmospheres Program under Grant NAG5-4190.

Appendix A

In this appendix we develop a model of microwave radiation from Venus. Similar developments can be found in many other places (see e.g., Barrett 1961; Gale and Sinclair 1972; Muhleman *et al.* 1979; Janssen and Klein 1981; Fahd and Steffes 1992; Gurwell *et al.* 1995). We first divide the atmosphere of Venus into N layers. We then trace rays (lines of sight) which intercept the atmosphere along their path to find the effective emission temperature as a function of position on the sky $T_b(x, y)$ (the sky brightness distribution). Throughout this treatment we will assume that we are in the Rayleigh-Jeans portion of the spectrum, so that the intensity B_ν is proportional to the brightness temperature T_b.

We find $T_b(x, y)$ by tracing the ray which intercepts the N^{th} (topmost) layer of the atmosphere at plane-of-sky position x, y downward through the layers until it either strikes the surface, or passes out of the back of the atmosphere. The technique is similar in many ways to those described in Hase and Höpfner (1999). The model uses cartesian coordinates x, y, and z, with the center of Venus at the origin, and the observer along the z-axis (at $z = \infty$). We define a ray as the set of points along a line:

$$\mathbf{r}(s) = \mathbf{a} + \mathbf{b}\, s \quad , \tag{12}$$

where $\mathbf{a}$ is the vector position of the starting point of the ray, $\mathbf{b}$ is a unit vector in the direction of the ray, and s is the distance along the ray. So, at the beginning of the ray trace for sky position (x, y), we set $\mathbf{a}_N = (x_N, y_N, z_N)$, where $x_N = x, y_N = y$, and $z_N = \sqrt{r_N^2 - x^2 - y^2}$, with r_N the radius of the upper boundary of the uppermost layer. The direction of the initial ray is: $\mathbf{b}_N = (0, 0, -1)$. We then calculate the distance to the next layer, s_N by performing

a ray-sphere intersection test (see e.g., Haines 1989) with the sphere being defined by the radius of the lower boundary of the uppermost layer. The ray in the N^{th} layer is now all points along the ray with $s < s_N$. Appropriate quantities for that layer are then calculated (see below). The starting point of the ray in the next layer down (the $N-1^{st}$ layer) is then defined by: $\mathbf{a}_{N-1} = \mathbf{a}_N + \mathbf{b}_N\, s_N$. To find the direction of the ray in the $N-1^{st}$ layer, we apply Snell's law, using the ratio of the indeces of refraction in the $N-1^{st}$ and N^{th} layers. We do this following the method of Heckbert (1989), noting that the incident ray ($\mathbf{I}$ in Heckbert) is $\mathbf{b}_N$, and the surface normal ($\mathbf{N}$ in Heckbert) is $\mathbf{a}_{N-1}/|\mathbf{a}_{N-1}|$. This procedure is repeated down through the layers, yielding the ray parameters for each layer: $\mathbf{a}_i, \mathbf{b}_i$, and s_i for layer i. The ray trace is continued down through the layers until either the surface of the planet is intersected, or the ray-sphere intersection indicates that the lower boundary of a layer is not intercepted. If the lower boundary is not intercepted, we know that this is a limb-sounding ray. In that case, a ray-sphere intersection is performed with the sphere being defined by the radius of the upper boundary of the layer. In order to test whether the ray intersects the surface or not, in each layer with radius below the maximum topographic radius measured by Magellan, a surface intersection test is done, based upon the topography at the longitude and latitude along the ray in that layer. If the surface is intersected in level l, then s_l is set as the distance from $\mathbf{a}_l$ to the surface intersection point. The topography as a function of position is taken from the Magellan GTDR data set (Plautt 1993).

For rays which strike the surface, the brightness temperature is composed of three elements:

$$T_b(x,y) = T_{atm}(x,y) + T_{emit}(x,y) + T_{refl}(x,y) \quad , \tag{13}$$

where T_{atm} is the atmospheric contribution to the emission, T_{emit} is the surface emission contribution, and T_{refl} is the contribution due to downward atmospheric emission which is reflected back up by the surface. The atmospheric term is a sum of the contribution from each atmospheric layer, attenuated by the opacity of all layers above it. This can be written:

$$T_{atm}(x,y) = \sum_{i=l}^{N} T_i(\gamma_i, \phi_i) \left(1 - e^{-\tau_{i,i}}\right) \; e^{-\tau_{i+1,N}} \quad , \tag{14}$$

where l is the layer in which surface intersection occurs, T_i is the average physical temperature of the i^{th} layer (which can be a function of, e.g., latitude), γ_i and ϕ_i are the planetary longitude and latitude of the i^{th} layer, given x and y, and $\tau_{b,c}$ is an opacity term. The quantity $(1 - e^{-\tau_{i,i}}) \; e^{-\tau_{i+1,N}}$ is called the *weighting function* for layer i. The opacity term is:

$$\tau_{b,c} = \sum_{a=b}^{c} \tau'_a \quad . \tag{15}$$

The opacity of the i^{th} layer, τ'_i, is obtained by integrating along the ray in the layer ($\mathbf{r}_i(s) = \mathbf{a}_i + \mathbf{b}_i \, s$):

$$\tau'_i = \int_0^{s_i} \; k(s) \, ds \quad , \tag{16}$$

where $k(s)$ is the total atmospheric absorption at position s along the ray. This integral equation for the opacity in each layer is solved numerically. The absorption is a sum over all species which contribute to the microwave opacity, which we here assume are only CO_2, SO_2, and H_2SO_4. We use the expression of Ho *et al.* (1966) for the absorption of CO_2 (in units of km^{-1}):

$$k_{\mathrm{CO_2}} = 2.65 \times 10^7 \; \nu_{GHz}^2 \; P^2 \; \left(\frac{1}{T}\right)^5 \; \left(f_{\mathrm{CO_2}}^2 + 0.25 f_{\mathrm{CO_2}} f_{\mathrm{N_2}} + 0.0054 f_{\mathrm{N_2}}^2\right) \quad , \tag{17}$$

where ν_{GHz} is the frequency in GHz, P is the pressure in atm, T is the temperature in K, $f_{\mathrm{CO_2}}$ is the molar fraction of CO_2, and $f_{\mathrm{N_2}}$ is the molar fraction of N_2. We use the expression

of Kolodner and Steffes (1998) for the absorption of H_2SO_4, with a slight modification of the coefficient (again in units of km^{-1}):

$$k_{H_2SO_4} = 2.176 \times 10^9 \ \nu_{GHz}^{1.15} \ P^{1.08} \ \left(\frac{1}{T}\right)^3 \ f_{H_2SO_4} \quad , \tag{18}$$

where $f_{H_2SO_4}$ is the molar fraction of H_2SO_4. We use the full formalism of Suleiman *et al.* (1996) for the absorption of SO_2, including 1587 lines of SO_2 below 750 GHz. All of these absorptions require knowledge of the temperature and pressure along the ray path. We assume that temperature varies linearly in the layers, and that pressure varies exponentially, allowing us to calculate these quantities at each point along the path.

We combine the contributions from the surface and subsurface emission and surface reflection of downward emission from the atmosphere into one term:

$$T_{emit}(x,y) + T_{refl}(x,y) = T_s'(\gamma_l, \phi_l) \ e^{-\tau_{l,N}} \quad , \tag{19}$$

where T_s' is the *effective* brightness temperature of the surface at the appropriate latitude and longitude. Again, this is a combination of surface and subsurface emission and reflection:

$$T_s'(\gamma_l, \phi_l) = R(\gamma_l, \phi_l) \, T_{\rm down}'(x,y) + T_s''(\gamma_l, \phi_l) \quad , \tag{20}$$

where $R(\gamma_l, \phi_l)$ is the Fresnel reflectivity of the surface at the wavelength of interest for the surface location where intersection occurs, $T_{\rm down}'(x,y)$ is the effective brightness temperature of the downward atmospheric radiation, and $T_s''(\gamma_l, \phi_l)$ is the effective brightness temperature resulting from the emission from the surface and subsurface for the given surface location. We use the two layer model of Tikhonova and Troitskii (1969) for the surface and subsurface emission:

$$T_s'' = \left(1 - R - R_2 \, e^{-2 \, \kappa \, a \, \sec e}\right) \ \left[T_s + \frac{q}{k \, \kappa \, \sec e'} \ \left(1 - e^{-\kappa \, a \, \sec e'}\right)\right] \quad , \tag{21}$$

where R_2 is the Fresnel reflectivity between the upper and lower subsurface layers, κ and k are the absorption coefficient and thermal conductivity in the upper layer, q is the heat flux from the interior of the planet, e is the emission angle from the upper layer into the atmosphere, e' is the emission angle from the lower layer into the upper layer, and T_s is the physical surface temperature. Note that the full model of Tikhonova and Troitskii (1969) allows for an additional term in this equation, involving the subsurface temperature gradient. Given the thermal insulation of the atmosphere, it is expected that the subsurface temperature gradient on Venus should be very small, and we have therefore not included that term here. Note also that R, R_2, e, e', and T_s are all functions of the surface location where ray intersection occurs. The surface temperature, T_s, is calculated based upon the topography at the location where the ray strikes the surface, and the temperature vs. radius information input to the model. The absorption coefficient (κ) is defined by:

$$\kappa = \frac{2\,\pi}{\lambda}\ \tan\delta'\ \sqrt{\epsilon_r} \quad , \tag{22}$$

where ϵ_r is the real part of the complex dielectric constant of the subsurface, and $\tan\delta'$ is the "specific loss tangent":

$$\tan\delta' = \frac{\tan\delta}{\rho\ (1-\omega)} = \frac{\epsilon_i/\epsilon_r}{\rho\ (1-\omega)} \quad , \tag{23}$$

where ρ is the subsurface density, ω accounts for subsurface scattering losses, ϵ_i is the imaginary part of the complex dielectric constant, and $\tan\delta'$ is the loss tangent ($\tan\delta = \epsilon_i/\epsilon_r$).

The surface reflectivity is (by averaging the reflectivities in the parallel (p) and perpendicular (s) polarizations):

$$R = \frac{|r_p|^2 + |r_s|^2}{2} \quad , \tag{24}$$

where r_q is the reflection coefficient for polarization q. These reflection coefficients are:

$$r_p = \frac{-n^2 \cos e + \sqrt{n^2 - \sin^2 e}}{n^2 \cos e + \sqrt{n^2 - \sin^2 e}} \quad , \tag{25}$$

and

$$r_s = \frac{\cos e - \sqrt{n^2 - \sin^2 e}}{\cos e + \sqrt{n^2 - \sin^2 e}} \quad , \tag{26}$$

where n is the ratio of the index of refraction of the surface material ($n_s \sim \sqrt{\epsilon_r}$ for a non-magnetic surface) to the index of refraction of the lowest atmospheric layer, and e is the emission angle (the angle between the incident ray and the surface normal). The real part of the dielectric constant of a surface with Fresnel reflectivity at normal incidence R_o is:

$$\epsilon_r = \left(\frac{1 + \sqrt{R_o}}{1 - \sqrt{R_o}} \right)^2 \quad . \tag{27}$$

The value of R_o as a function of location on Venus is taken from the GREDR data set (Plautt 1993). The effective brightness temperature of the downward atmospheric radiation is given by:

$$T'_{\rm down} = T_{CMB}\ e^{-\tau_{l,N}} + \sum_{i=l}^{N} T_i(\gamma_i, \phi_i)\ \left(1 - e^{-\tau_{i,i}}\right)\ e^{-\tau_{l,i-1}} \quad , \tag{28}$$

where T_{CMB} is the cosmic microwave background temperature, taken to be 2.7 K.

For rays which do not strike the surface (limb sounding rays), the effective brightness temperature is composed only of atmospheric elements:

$$T_b(x, y) = T_{atm}(x, y) + T'_{atm}(x, y) \quad , \tag{29}$$

where the first term is the same as for the rays which strike the surface (Eq. 14), and the second term accounts for the emission from the back side of the atmosphere. This back side

contribution is:

$$T'_{atm}(x,y) = \sum_{i=l}^{N} T_i(\gamma_i, \phi_i) \left(1 - e^{-\tau_{i,i}}\right) \; e^{-\left(\tau_{l,N} + \tau_{l,i-1}\right)} \quad . \tag{30}$$

Note that care must be taken in treating the lowest layer correctly. We do this by taking the ray through that layer, and dividing it in two, and taking the radius of that halfway point along the ray as the lower radius of the lowest layer. The average temperature of that lowest layer is then adjusted appropriately (assuming linear temperature variation).

The required inputs to the model are quantities as a function of altitude for the atmosphere, and values for the surface quantities as a function of position on Venus. As previously stated, the surface quantities (topography and dielectric constant) are taken from the GTDR and GREDR Magellan data sets (Plautt 1993). The necessary atmospheric quantities are: pressure, temperature, and the molar fraction of the atmospheric constituents (CO_2, N_2, SO_2, H_2SO_4). Given the other inputs, the index of refraction is calculated in each layer via:

$$n_i = 1.0 + 0.1329 \, \frac{P}{T} \quad . \tag{31}$$

Given the ability to calculate the brightness temperature as a function of position, the average brightness temperature is then obtained by integration over the sky coordinates (see Eq. 6). It is common to assume azimuthal symmetry, to reduce Eq. 6 to:

$$\overline{T_b} = 2 \int_0^1 T_b(\rho) \, \rho \, d\rho \quad , \tag{32}$$

for radial coordinate $\rho = r/R$. We do not take this step, in order to take into account the variations in the surface and atmospheric properties across the disk. We solve the full 2-D integral in Eq. 6 numerically.

Appendix B

In this appendix we derive the correction due to resolution of Venus in the primary beam of the antennas of the VLA. The theoretical antenna response of the VLA is circularly symmetric, and is given by (Napier, 1999):

$$A(u) = |F(u)|^2 \quad , \tag{33}$$

where:

$$F(u) = \frac{J_1(2\pi a u)}{\pi\, a\, u} \quad . \tag{34}$$

J_1 is the Bessel function of the first kind, order 1, a is the physical radius of the antenna (in meters), and u is the angle on the sky in wavelengths, i.e., $u = \theta/\lambda$, for sky distance θ in radians, and wavelength λ. For this theoretical primary beam, the full width half maximum (FWHM) as a function of wavelength is given by:

$$\theta_A = \frac{1.03\,\lambda}{2\,a} \text{ radians} \quad \sim \frac{42.42}{\nu_{GHz}} \text{ arcmin} \quad , \tag{35}$$

where ν_{GHz} is the frequency in GHz. The measured FWHM of the VLA antennas is well described by this relation. Using the data of Napier and Rots (1982), and fitting a primary beam like equation 34 for the FWHM yields $\theta_A \sim 44.43/\nu_{GHz}$. Note that Napier and Rots (1982) derive $\theta_A \sim 44.26/\nu_{GHz}$, but use a polynomial approximation to the primary beam shape rather than the more accurate Besselian shape. Table B.I shows the value of θ_A calculated using equation 35 for the wavelengths of our observations. This table also shows the size of the planet during our observations. It is apparent that some reduction in the detected flux density may occur due to resolution of Venus by the primary beam. We wish

to correct for that reduction by calculating a correction factor, C, such that the *true* flux density (S_ν, see equation 5) is related to the *detected* flux density (S'_ν) by:

$$S_\nu = \frac{S'_\nu}{C} \quad . \tag{36}$$

So, given an observed source large enough such that $A(u)$ is significantly < 1 over some part of it, what is the reduction in flux density for a VLA antenna? Assuming circular symmetry, the ratio of the detected to true flux density is:

$$C = \frac{S'_\nu}{S_\nu} = \frac{\int_0^{u_{max}} A(u)\, B(u)\, u\, du}{\int_0^{u_{max}} B(u)\, u\, du} \quad , \tag{37}$$

where $B(u)$ is the source brightness distribution (assumed circularly symmetric), and u_{max} is the source size in wavelengths, i.e., $u_{max} = R/\lambda$ for a source of angular radius R. For the source distribution presented in the Modeling section ($B(u) = B_o \cos^n(u/u_{max})$), this becomes:

$$C = (2+n)\left(\frac{\lambda}{R}\right)^2 \int_0^{R/\lambda} A(u)\, \cos^n\left(\frac{u\lambda}{R}\right) u\, du \quad . \tag{38}$$

Unfortunately this integral must be evaluated numerically. Table B.I shows the resultant modified correction factor, expressed as a percent change in the flux density (i.e., $C' = 100\,(1-C)\,\%$), given the value of n derived from the fits. Also shown in Table B.I are values of C' calculated using $n = 0$ and $n = 1$, to illustrate that the value of C' (and C) is not particularly sensitive to variations in n, for our observations. Inspection of Table B.I shows that the correction is only $> 1\%$ for the highest frequency (22.46 GHz). However, since we know what the correction factor should be we still apply it at the longer wavelengths, even though the it is $< 1\%$.

References

Allen, D.A., and J.W. Crawford 1984. Cloud Structure on the Dark Side of Venus. *Nature* **307**, 222–224.

Baars, J.W.M., R. Genzel, I.I.K. Pauliny–Toth, and A. Witzel 1977. The Absolute Spectrum of Cas A; An Accurate Flux Density Scale and a Set of Secondary Calibrators. *Astron. Astrophys.* **61**, 99–106.

Barrett, A.H. 1961. Microwave Absorption and Emission in the Atmosphere of Venus. *Astrophys. J.* **133**, 281–293.

Barrett, A.H., and D.H. Staelin 1964. Radio Observations of Venus and the Interpretations. *Space Sci. Rev.* **3**, 109–135.

Berge, G.L., and E.W. Greisen 1969. High–Resolution Interferometry of Venus at 3.12–cm Wavelength. *Astrophys. J.* **156**, 1125–1134.

Berge, G.L., D.O. Muhleman, and G.S. Orton 1972. High Resolution Interferometric Observations of Venus at Three Radio Wavelengths. *Icarus* **17**, 675–681.

Bézard, B., C. deBergh, B. Fegley, J.-P. Maillard, D. Crisp, T. Owen, J.B. Pollack, and D. Grinspoon 1993. The Abundance of Sulfur Dioxide Below the Clouds of Venus. *Geophys. Res. Lett.* **20**, 1587–1590.

Blamont, J., L. Boloh, V. Kerzhanovich, L. Kogan, M. Kurgansky, V. Linkin, L. Matveenko, M. Roy, D. Patsaev, *et al.* 1993. Balloons on Planet Venus – Final Results. *Adv. Space Res.* **13**, 145–152.

Butler, B.J., and T.S. Bastian 1999. Solar System Objects. In *Synthesis Imaging in Radio Astronomy II* (G.B. Taylor, C.L. Carilli, and R. A. Perley, Eds.) pp. 625–656. Astronomical Society of the Pacific Conference Series, San Francisco.

Clark, B.G., and C.L. Spencer 1964. Some Decimeter Observations of Venus During the 1962 Conjunction. *Astron. J.* **69**, 59–61.

Clark, B.G., and A.D. Kuz'min 1965. The Measurement of the Polarization and Brightness Distribution of Venus at 10.6–cm Wavelength. *Astrophys. J.* **142**, 23–44.

Cornwell, T.J., and E.B. Fomalont 1999. Self–Calibration. In *Synthesis Imaging in Radio Astronomy II* (G.B. Taylor, C.L. Carilli, and R. A. Perley, Eds.) pp. 187–199. Astronomical Society of the Pacific Conference Series, San Francisco.

Crisp, D., D.A. Allen, D.H. Grinspoon, and J.B. Pollack 1991. The Dark Side of Venus: Near Infrared Images and Spectra from the Anglo–Australian Observatory. *Science* **253**, 1263–1266.

Esposito, L.W., M. Copley, R. Eckert, L. Gates, A.I.F. Stewart, and H. Worden 1988. Sulfur Dioxide at the Venus Cloud Tops. 1978–1986, *J. Geophys. Res.* **93**, 5267–5276.

Fahd, A.K., and P.G. Steffes 1992. Laboratory Measurements of the Microwave and

Millimeter–Wave Opacity of Gaseous Sulfur Dioxide (SO_2) under Simulated Conditions for the Venus Atmosphere. *Icarus* **97**, 200–210.

Florenskii, K.P., and 9 others 1982. Analysis of the Panoramas of the Venera 13 and Venera 14 Landing Sites. *Sov. Astron. Lett.* **8**, 233–234.

Ford, P.G., and G.H. Pettengill 1992. Venus Topography and Kilometer–Scale Slopes. *J. Geophys. Res.* **97**, 13103–13114.

Gurwell, M.A., D.O. Muhleman, K.P. Shah, G.L. Berge, D.J. Rudy, and A.W. Grossman 1995. Observations of the CO Bulge on Venus and Implications for Mesospheric Winds. *Icarus* **115**, 141–158.

Hall, R.W., and N.J.B.A. Branson 1971. High Resolution Radio Observations of the Planet Venus at a Wavelength of 6 cm. *Mon. Not. Roy. Astron. Soc.* **151**, 185–196.

Haines, E. 1989. Essential Ray Tracing Algorithms. In *An Introduction to Ray Tracing* (A.S. Glassner, Ed.) pp. 33–77. Academic Press, New York.

Hase, F., and M. Höpfner 1999. Atmospheric Ray Path Modeling for Radiative Transfer Algorithms. *Appl. Opt.* **38**, 3129–3133.

Heckbert, P.S. 1989. Writing a Ray Tracer. In *An Introduction to Ray Tracing* (A.S. Glassner, Ed.) pp. 263–293. Academic Press, New York.

Ho, W., I.A. Kaufman, and P. Thaddeus 1966. Laboratory Measurement of Microwave Absorption in Models of the Atmosphere of Venus. *J. Geophys. Res.* **71**, 5091–5108.

Janssen, M.A., and M.J. Klein 1981. Constraints on the Composition of the Venus Atmosphere from Microwave Measurements near 1.35 cm Wavelength. *Icarus* **46**, 58–69.

Jenkins, J.M., and P.G. Steffes 1991. Results for 13–cm Absorptivity and H_2SO_4 Abundance Profiles from the Season 10 (1986) Pioneer Venus Orbiter Radio Occultation Experiment. *Icarus* **90**, 129–138.

Jenkins, J.M., P.G. Steffes, D.P. Hinson, J.D. Twicken, and G.L. Tyler 1994. Radio Occultation Studies of the Venus Atmosphere with the Magellan Spacecraft 2. Results from the October 1991 Experiments. *Icarus* **110**, 79–94.

Jenkins, J.M., B.J. Butler, P.G. Steffes, and M.A. Kolodner 1998. Retrievals of Sulfur–Bearing Gas Abundances from Microwave Emission Maps of Venus Obtained at the VLA. *BAAS* **30**, 1449.

Jenkins, J.M., M.A. Kolodner, S.H. Suleiman, B.J. Butler, and P.G. Steffes 2000. The Distribution of Sulfur–Bearing Compounds in the Lower Venus Atmosphere. in preparation.

Kolodner, M.A., and P.G. Steffes 1998. The Microwave Absorption and Abundance of Sulfuric Acid Vapor in the Venus Atmosphere based on New Laboratory Measurements. *Icarus* **132**, 151–169.

Lecacheux, L., P. Drossart, P. Laques, F. Deladerrière, and F. Colas 1993. Detection of the Surface fo Venus at 1.0 μm from Ground–Based Observations. *Planet. Space Sci.* **41**, 543–549.

McGovern, P.J., M. Simons, and S.C. Solomon 1995. Estimates of Elastic Lithosphere Thickness and Heat Flux Beneath Large Volcanoes on Venus. *LPSC XXVI*, 941–942.

Muhleman, D.O., G.L. Berge, and G.S. Orton 1973. The Brightness Temperature of Venus and the Absolute Flux–Density Scale at 608 MHz, *Astrophys. J.* **183**. 1081–1085.

Muhleman, D.O., G.S. Orton, and G.L. Berge 1979. A Model of the Venus Atmosphere from Radio, Radar, and Occultation Observations. *Astrophys. J.* **234**, 733–745.

Na, C.Y., L.W. Esposito, and T.E. Skinner 1990. International Ultraviolet Explorer Observation of Venus SO_2 and SO. *J. Geophys. Res.* **95**, 7485–7491.

Na, C.Y., L.W. Esposito, W.E. McClintock, and C.A. Barth 1994. Sulfur Dioxide in the Atmosphere of Venus II. Modeling Results. *Icarus* **112**, 389–395.

Napier, P. 1999. The Primary Antenna Elements. In *Synthesis Imaging in Radio Astronomy II* (G.B. Taylor, C.L. Carilli, and R.A. Perley, Eds.) pp. 37–56. Astronomical Society of the Pacific Conference Series, San Francisco.

Napier, P., and A. Rots 1982. VLA Primary Beam Parameters. VLA Test Memo No. 134, NRAO.

Oyama, V.I., G.C. Carle, J. Woeller, J.B. Pollack, R.T. Reynolds, and R.A. Craig 1980. Pioneer Venus Gas Chromotography of the Lower Atmosphere of Venus. *J. Geophys. Res.* **85**, 7891–7902.

Pettengill, G.H., P.G. Ford, and B.D. Chapman 1988. Venus: Surface Electromagnetic Properties. *J. Geophys. Res.* **93**, 14881–14892.

Pettengill, G.H., P.G. Ford, W.T.K. Johnson, R.K. Raney, and L.A. Sauderblom 1991. Magellan: Radar Performance and Data Products. *Science* **252**, 260–265.

Pettengill, G.H., P.G. Ford, and R.J. Wilt 1992. Venus Surface Radiothermal Emission as Observed by Magellan. *J. Geophys. Res.* **97**, 13091–13102.

Plautt, J.J. 1993. The Non–SAR Experiments. In *Guide to Magellan Image Interpretation* pp. 19–31, JPL Publication 93–24.

Saunders, R.S., *et al.* 1992. Magellan Mission Summary. *J. Geophys. Res.* **97**, 13067–13090.

Schloerb, F.P., D.O. Muhleman, and G.L. Berge 1976. Lunar Heat Flow and Regolith Structure Inferred from Intererometric Observations at a Wavelength of 49.3 cm. *Icarus* **29**, 329–341.

Sieff, A. 1991. Atmospheres of Earth, Mars, and Venus, as Defined by Entry Probe Experiments. *J. Space. Rock.* **28**, 265–275.

Sinclair, A.C.E., J.P. Basart, D. Buhl, and W.A. Gale 1972. Precision Interferometric Observations of Venus at 11.1–Centimeter Wavelength. *Astrophys. J.* **175**, 555–572.

Steffes, P.G., M.J. Klein, and J.M. Jenkins 1990. Observations of the Microwave Emission of Venus from 1.3 to 3.6 cm. *Icarus* **84**, 83–92.

Steffes, P.G., J.M. Jenkins, R.S. Austin, S.W. Asmar, D.T. Lyons, E.H. Seale, and G.L. Tyler 1994. Radio Occultation Studies of the Venus Atmosphere with the Magellan Spacecraft 1. Experimental Description and Performance. *Icarus* **110**, 71–78.

Suleiman, S.H., M.A. Kolodner, and P.G. Steffes 1996. Laboratory Measurement of the Temperature Dependence of Gaseous Sulfur Dioxide (SO_2) Microwave Absorption with Application to the Venus Atmosphere. *J. Geophys. Res.* **101**, 4623–4635.

Thompson, A.R., J.M. Moran, and G.W. Swenson Jr. 1991. *Interferometry and Synthesis in Radio Astronomy*, Krieger Publishing Co., Malabar.

Tikhonova, T.V., and V.S. Troitskii 1969. Effect of Heat from Within the Moon on its Radio Emission for the Case of Lunar Properties which Vary with Depth. *Sov. Astron. AJ* **13**, 120–128.

Turegano. J.A., and M.J. Klein 1980. Calibration Radio Sources for Radio Astronomy: Precision Flux Density Measurements at 8420 MHz. *Astron. Astrophys.* **86**, 46–49.

Tyler, G.L., R.A. Simpson, M.J. Maurer, and E. Holmann 1992. Scattering Properties of the Venusian Surface: Preliminary Results from Magellan. *J. Geophys. Res.* **97**, 13115–13139.

Vinogradov, A.P., K.P. Florenskii, A.T. Bazilevskii, and A.S. Selivanov 1976. First panoramic pictures of Venus: preliminary image analysis. *Sov. Astron. Lett.* **2**, 67–71.

Zasova, L.V., V.I. Moroz, L.W. Esposito, and C.Y. Na 1993. SO_2 in the Middle Atmosphere of Venus: IR Measurements from Venera–15 and Comparison to UV Data. *Icarus* **105**, 92–109.

Table I. Ephemeris information for Venus observations.

date (1996)	time range (IAT)	RA	Dec	D (AU)	phase angle	frequencies (GHz)	VLA config
April 05	1645–2747	03:57:16.65	+24:04:23.2	0.6735	92	14.94, 22.46	C
April 30	0148–0224	05:21:46.50	+27:39:02.8	0.4862	112	4.86, 8.44	C

Table II. Calibrators.

date (1996)	frequency (GHz)	primary calibrator, flux density	secondary calibrator, flux density
April 05	22.46	3C286, 2.498 Jy	0403+260, 0.562 Jy
April 05	14.94	3C286, 3.428 Jy	0403+260, 0.642 Jy
April 30	8.44	3C286, 5.189 Jy	0555+398, 5.943 Jy
April 30	4.86	3C286, 7.486 Jy	0555+398, 5.951 Jy

Table III. Fit values.

frequency (GHz)	V_o (Jy)	$\overline{T_b}^*$ (K)	n
22.46	88.860 ± 0.004	505.2 ± 25.3	0.161
14.94	44.454 ± 0.001	565.9 ± 17.0	0.151
8.44	31.736 ± 0.002	657.5 ± 13.2	0.096
4.86	10.915 ± 0.001	679.9 ± 13.6	0.019

* includes primary beam correction (see appendix B), and uncertainty in flux density calibration scale.

Table B.I. Correction factors for primary beam resolution.

frequency (GHz)	θ (Venus)	θ_A (arcsec)	C' (%)	$C'(n=0)$ (%)	$C'(n=1)$ (%)
22.46	12.53	119	1.57	1.60	1.44
14.94	12.53	178	0.69	0.71	0.63
8.44	17.36	316	0.44	0.44	0.40
4.86	17.36	548	0.15	0.15	0.13

B.J. Butler *et al.* – Figure 1.

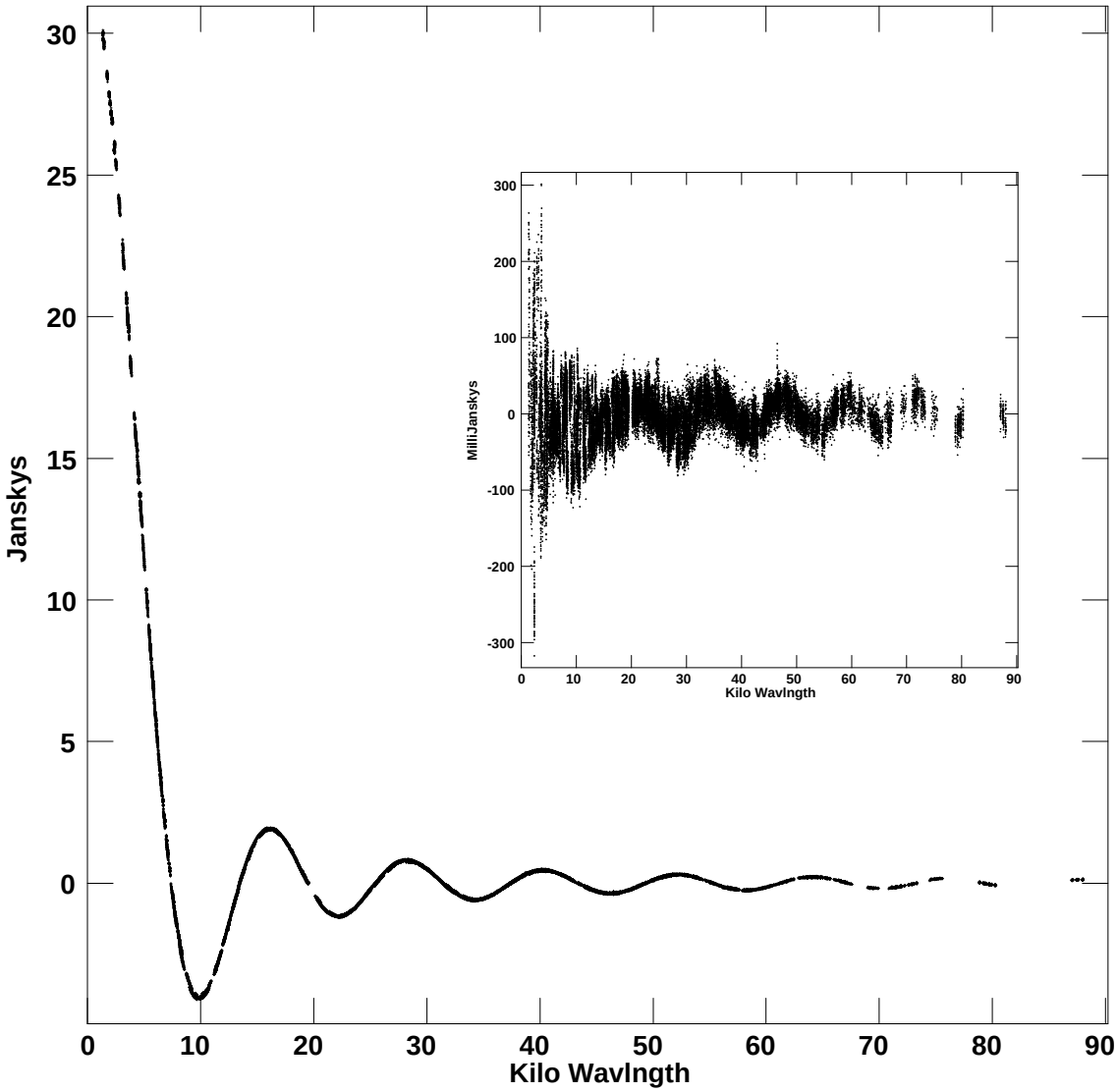

Figure 1. Measured visibilities from Venus at 8.44 GHz as a function of baseline length (in wavelengths). Shown in the inset are the residuals after the best-fit circularly symmetric model was subtracted.

B.J. Butler *et al.* – Figure 2.

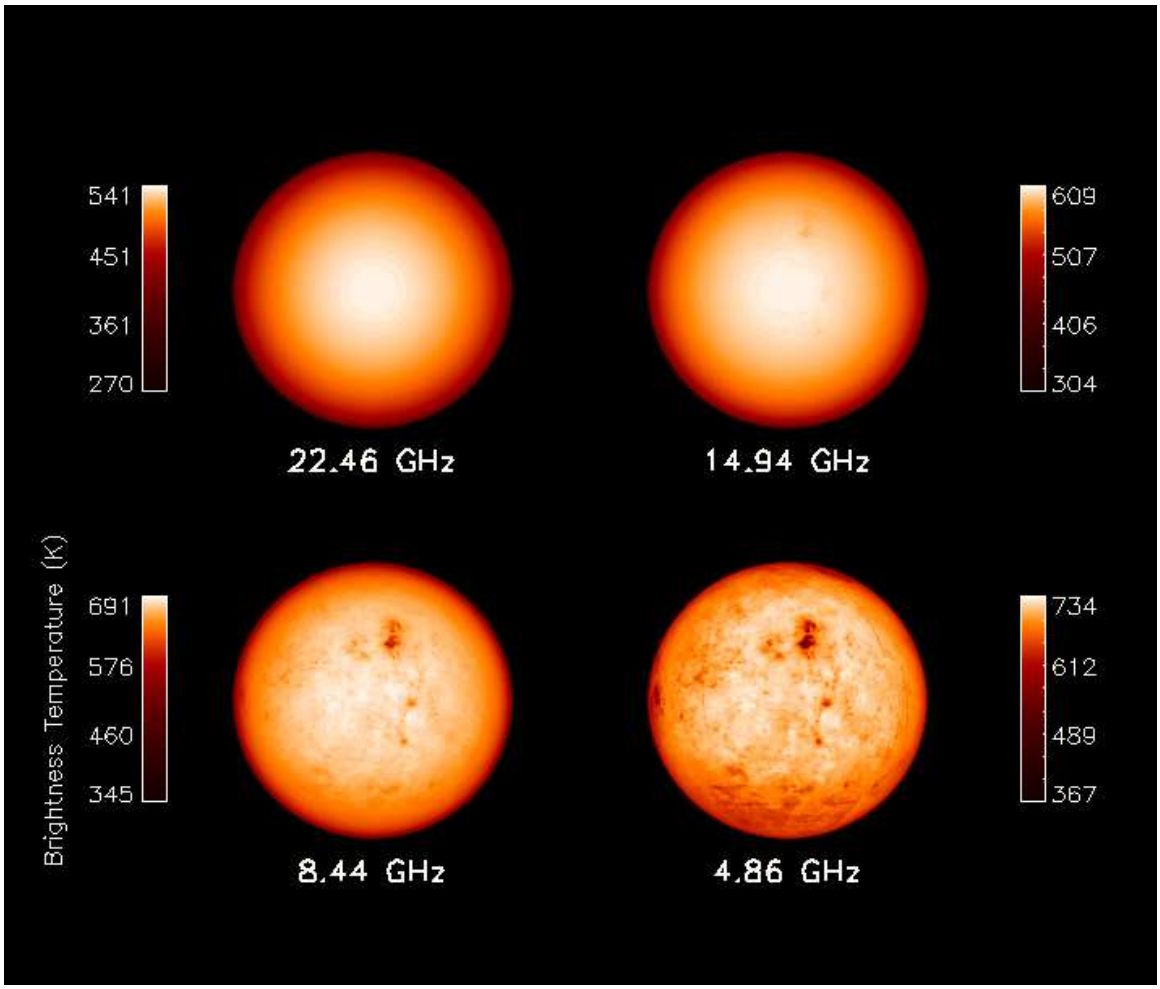

Figure 2. Maps of the model brightness temperature distributions at the four frequencies.

B.J. Butler *et al.* – Figure 3.

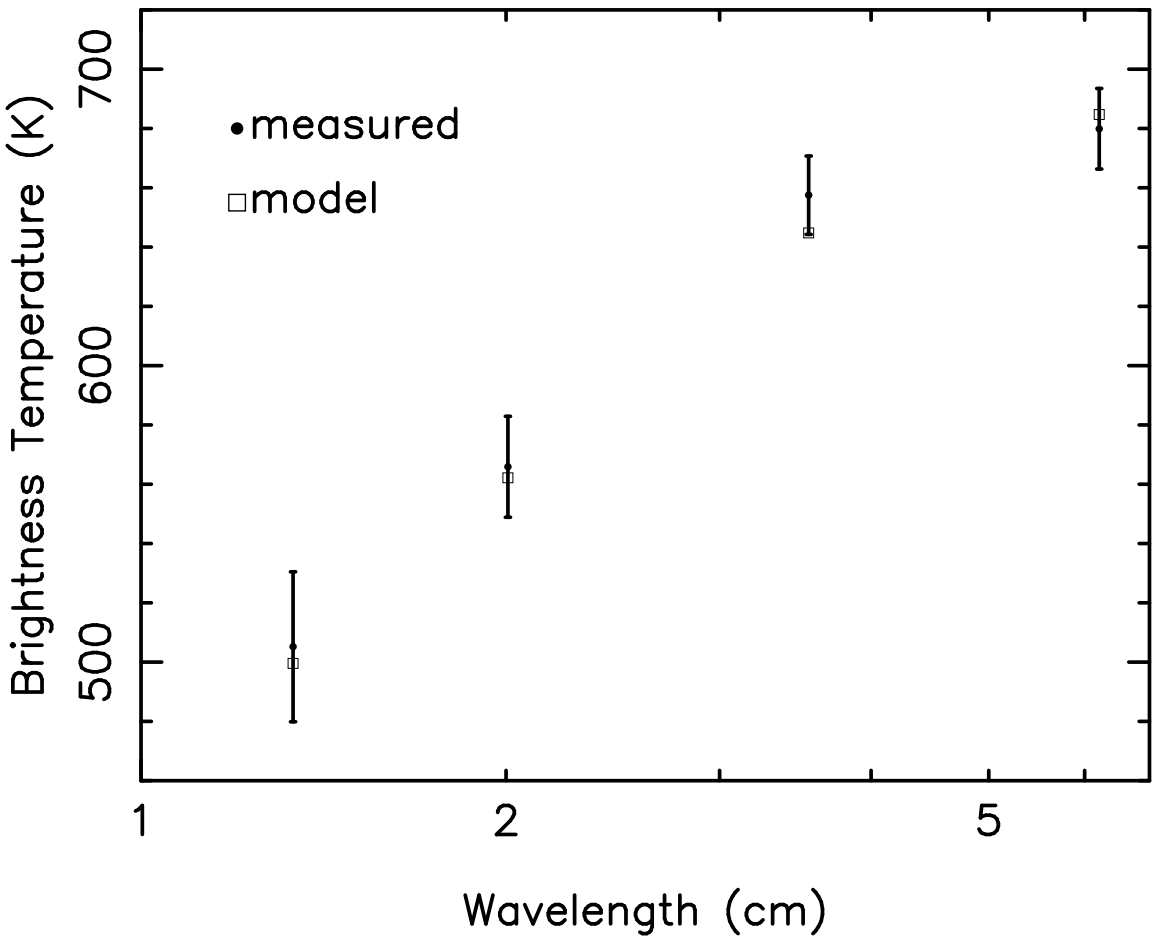

Figure 3. Derived disk averaged brightness temperature for Venus for the four wavelengths presented here. Also shown are the model values at the same wavelengths.